CANCER

Measuring competitive exclusion in non–small cell lung cancer

Nathan Farrokhian[1]†, Jeff Maltas[2]†, Mina Dinh[2], Arda Durmaz[1], Patrick Ellsworth[1], Masahiro Hitomi[2], Erin McClure[2], Andriy Marusyk[3], Artem Kaznatcheev[4]*, Jacob G. Scott[1,2,5]*

In this study, we experimentally measure the frequency-dependent interactions between a gefitinib-resistant non–small cell lung cancer population and its sensitive ancestor via the evolutionary game assay. We show that cost of resistance is insufficient to accurately predict competitive exclusion and that frequency-dependent growth rate measurements are required. Using frequency-dependent growth rate data, we then show that gefitinib treatment results in competitive exclusion of the ancestor, while the absence of treatment results in a likely, but not guaranteed, exclusion of the resistant strain. Then, using simulations, we demonstrate that incorporating ecological growth effects can influence the predicted extinction time. In addition, we show that higher drug concentrations may not lead to the optimal reduction in tumor burden. Together, these results highlight the potential importance of frequency-dependent growth rate data for understanding competing populations, both in the laboratory and as we translate adaptive therapy regimens to the clinic.

INTRODUCTION

Given our current understanding of intratumoral heterogeneity, treatment resistance after continuous drug dose is an expected consequence. Genomic instability (*1*), inherent to the development of most cancer (*2*–*5*), results in the accumulation of a variety of aberrations within a single tumor population (*6*). While only a small subset of these randomly distributed changes will contribute directly to driving carcinogenesis, this diverse population composed of phenotypically distinct subclones results in increased resilience of the overall tumor population across a wide range of external stressors (*7*, *8*).

These distinct subclones do not live, grow, or reproduce in isolation, however. With this diverse cellular population comes a diverse range of intercellular interactions including competition (*9*) and cooperation between cancer cells (*10*) and complex interactions with the microenvironment (*11*–*13*). Complex systems cannot often be fully described empirically, and their dynamics can be difficult to intuit from measurements of their parts. In these situations, mathematical models have historically played a role. Specifically, evolutionary game theory has been effective in predicting the evolutionary consequences of interactions in large multicellular ecosystems, such as fisheries (*14*) and game reserves (*15*). More recently, these evolutionary game theoretical models have been used to gain insight into phenotypic shifts that occur within tumor ecosystems (*12*, *16*–*18*). As a consequence, we must understand both the absolute fitness advantages of particular subpopulations in the selecting environment (monoculture) and how competing clones modulate that advantage as a function of population frequency (coculture) (*19*). This frequency-dependent growth can drastically expand what challenges evolution can adapt to (*20*) and acts to shape treatment-naïve tumor ecosystems and influences inevitable development of resistance in posttreatment environments (*9*, *21*–*23*). As traditional treatment protocols continue to fail, more evolutionary-based treatments that rely on judicious treatment schedules and cooperative dynamics between populations have gained in popularity (*11*, *24*–*33*).

Dynamic therapeutic protocols using models of this type have already made their way into the clinic with promising results (*27*). While this highlights the value of game theoretical models for treatment optimization, the specific model in this and other clinical trials has been selected and parameterized mainly on the basis of biological conjecture and intuition (*34*, *35*). Instead, for each clinical condition, a different model and parameters would likely be needed to accurately capture intratumoral dynamics. Hence, the reproducibility of this initial success across different tissues and environmental contexts is contingent on our ability to measure subclonal interactions in the laboratory before transitioning to clinical practice. These interactions can greatly influence the evolutionary trajectory of the tumor; therefore, incorrect characterization could unintentionally worsen treatment outcomes.

One such concept that is frequently assumed to be the driver of inevitable treatment resistance within these models is that of competitive release (*36*). This phenomenon was first described by Connell (*37*) while studying the distribution of barnacles off the shore of Millport, Scotland, where it was observed that two species occupied two distinct horizontal zones on the shoreline. Connell determined that the upper species, *Chthamalus stellatus*, was competitively excluded from populating the lower region as a result of competitive interactions with the lower species, *Balanus balanoides*. The experimental removal of *Balanus* by Connell released *Chthamalus* from this competitive exclusion, which resulted in expansion into the lower horizontal zone. Similarly, in tumors, it is thought that selective killing of sensitive cells during therapy removes competitive restrictions on resistant populations, allowing for their outgrowth and subsequent therapeutic failure. While intuitive in theory and observed in bacteria (*38*) and parasites (*39*–*41*), the empirical evidence of the dynamics that underlie this phenomenon in cancer has, to our knowledge, yet to be elucidated.

As a population becomes increasingly resistant to a treatment, it is common for that population to pay a "fitness cost" to maintain

[1]CWRU School of Medicine, Cleveland, OH, USA. [2]Department of Translational Hematology and Oncology Research, Cleveland Clinic, Cleveland, OH, USA. [3]Department of Cancer Physiology, Moffitt Cancer Center, Tampa, FL, USA. [4]Department of Biology, University of Pennsylvania, Philadelphia, PA, USA. [5]Department of Radiation Oncology, Cleveland Clinic, Cleveland, OH, USA.
*Corresponding author. Email: scottj10@ccf.org (J.G.S.); kaznatcheev.artem@gmail.com (A.K.)
†These authors contributed equally to this work.

that resistant mechanism, leading to a reduced growth rate when compared to the ancestor from which it was derived (*42*, *43*). This has led many researchers to suggest that the sensitive ancestor is likely to outcompete the resistant clone when selection is removed, and thus, treatment holidays may be beneficial to the maintenance of a treatable cancer population (*12*, *27*). In some cases, the fitness cost may be competitive enough to result in competitive exclusion of the resistant strain upon treatment withdrawal. In this work, we consider the importance of empirical, frequency-dependent growth rate measurements in identifying competitive exclusion. Beginning with PC9, a model cancer system for epidermal growth factor receptor (*EGFR*) tyrosine kinase inhibitor resistance in non–small cell lung cancer (NSCLC), we show that competitive exclusion requires one population to outcompete (have a higher growth rate than) another population under all possible population frequencies. We then measure these frequency-dependent growth rates for a gefitinib-resistant population and the ancestor from which it was derived and show that competitive exclusion is likely but not guaranteed. We then show that the addition of gefitinib shifts the frequency-dependent growth rates such that the resistant strain will competitively exclude the ancestor at all tested concentrations. Last, combining our empirically derived growth measurements with traditional competition simulations, we demonstrate that the inclusion of ecological effects can significantly alter the predicted time to exclusion of the ancestor and thus alter the time required to reach an untreatable resistant tumor. In addition, we show that, contrary to the maximal tolerable dose hypothesis, higher drug doses may not constrain tumor burden better than lower doses for our system.

RESULTS

Ecological interactions ameliorate some but not the entire fitness cost associated with resistance, resulting in competitive exclusion of the resistant population in the absence of treatment

We investigated the evolutionary games (frequency-dependent ecological interactions) between sensitive and gefitinib-resistant cell lines in the lung adenocarcinoma cell line PC9. To create the resistant line, we exposed the population to 1 μM gefitinib for 6 months. In parallel, the original sensitive PC9 cell line was propagated in a matched volume of dimethyl sulfoxide (DMSO) for 6 months. To recapitulate the clinical scenario, upfront treatment with high escalated dose was chosen over dose escalation protocol. We then used the game assay that we have previously developed to quantify ecological interactions between populations (*30*). Briefly, we cocultured the derived gefitinib-resistant cell line with the DMSO-propagated sensitive cell line at varying sensitive population–to–resistant population ratios (Fig. 1A) in a 96-well plate. Using an automated incubator (BioTek BioSpa) and time-lapse microscopy setup, we imaged the wells every 4 hours. Cell lines were transduced with enhanced green fluorescent protein (EGFP) and mCherry fluorescent proteins that, when combined with image processing software, allowed for quantification of population-level cell counts and therefore population growth rates (Fig. 1B). Then, by combining the parallel experiments done at varying initial sensitive populations, we can plot the frequency-dependent growth rates for both the resistant and sensitive cell lines (Fig. 1C). Last, we can extract the payoff matrix that describes the evolutionary game dynamics as shown in Fig. 1D.

In addition to the frequency-dependent growth rate measurements based on heterogeneous (mixed sensitive and resistant populations), we also performed the more standard measure of the homogeneous monotypic growth rates for both cell lines in DMSO. In this case, there is a substantial growth cost to the resistant phenotype, which grows at roughly three-fourths (75.6%) the rate of the monotypic sensitive PC9 population (Fig. 2B, left). Fitness costs are often assumed in treatment-resistant populations of *EGFR*-driven NSCLC (*44*); however, this feature may not be generalizable across all NSCLC types (*30*). While it is tempting to extrapolate these data and suggest that these growth rate differences necessitate competitive exclusion of the resistant cell line due to its lower growth in DMSO, this is not necessarily so. Ecological interactions between the populations can ameliorate the fitness cost associated with resistance as shown in the left panel of the cartoon plot in Fig. 2A. The difference between the resistant and ancestor population's frequency-dependent growth rate is known as the gain function. For competitive exclusion to occur, the value of the gain function cannot change the sign for any population frequency. That is, if the gain function is positive (or negative), then it must remain positive (or negative) for all population frequencies. If instead the gain function transitions from negative to positive or vice versa, then a fixed point will occur (*45*). If the fixed point is stable (negative to positive gain), then it will allow for coexistence of both populations, while the opposite (positive to negative gain) leads to an unstable fixed point.

Our experiments reveal that the ancestor outcompetes the resistant population at all population frequencies, likely resulting in a complete competitive exclusion of the resistant population (Fig. 2B, right). To confirm that these were not a result of density-dependent growth effects (analogous to the inoculum effect in antibiotic resistance) (*46*), we measured the monoculture growth of both the sensitive and resistant population across a series of twofold dilutions (figs. S1 and S4). However, our coculture experiments indicate the opposite—the resistant population grows significantly faster at lower resistant population densities, suggesting that the observed coculture effects are not due to density-dependent monoculture interactions. In addition, using the raw growth data, we show that the coculture data are not well fit by a model of exponential growth that ignores ecological dynamics (figs. S2 and S3). In both populations, increasing density resulted in a slightly positive effect on growth.

However, the fitness cost of the resistant population is almost entirely ameliorated by ecological interactions occurring at high-sensitive population frequencies. Because this interaction occurs at resistant population fractions near zero that are hard to reliably measure empirically, it is possible that the resistant population is not completely competitively excluded, and a fixed point may exist at this extreme. If this were to be the case, then it could highlight one potential way a sensitive population may generate and maintain drug-resistant populations without losing population-level fitness, as the resistant strain with a significantly fitness cost could be maintained at low population frequency in the absence of drug.

The addition of drug switches which population is competitively excluded

Next, we sought to quantify the ecological interaction between the sensitive and resistant cell lines under the application of increasing gefitinib concentrations (Fig. 3A and fig. S5). We see that as the concentration of gefitinib increases, the slopes of the frequency-dependent growth rates (and therefore, ecological interaction magnitude) also

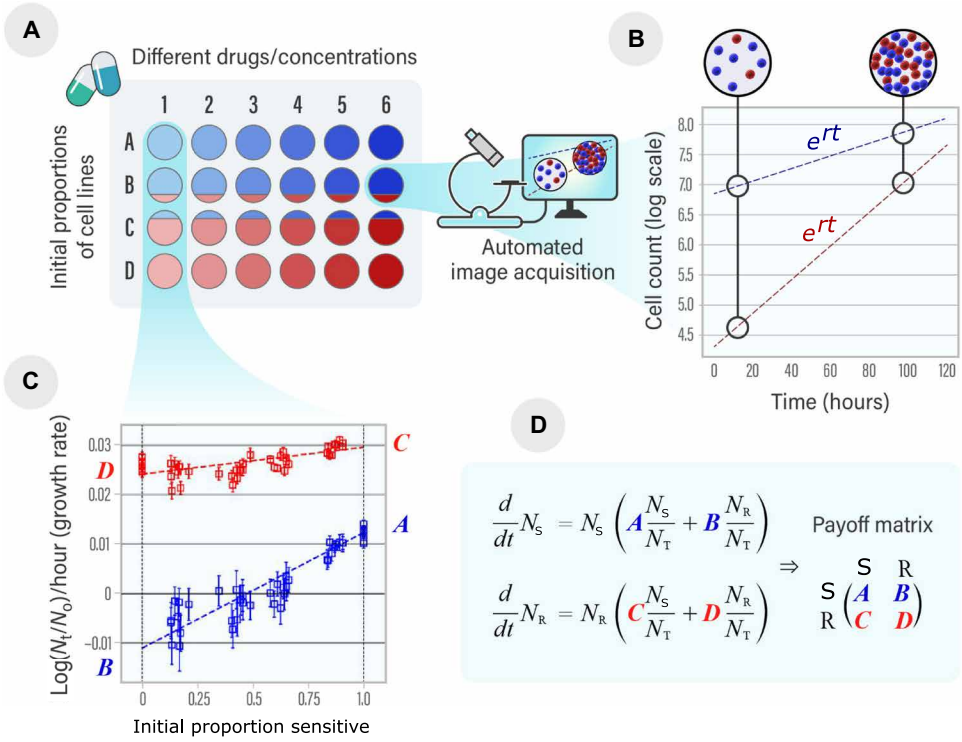

Fig. 1. Experimental design for evolutionary game assay. (**A**) To track differential growth dynamics of two populations in the same culture, each population was transduced with a vector encoding a different heritable fluorescent protein. A gefitinib-resistant cell line (red) and its sensitive ancestor (blue) were plated across a full spectrum of initial proportions (A, B, C, D...) and in a range of different drugs and concentrations (1, 2, 3, 4...) in a 96-well plate. (**B**) Automated time-lapse microscopy imaging captures the composition of the population in each well every 4 hours. Cell number counts were extracted from each fluorescent image and plotted against elapsed time to derive growth rates in each well for each population via semi-log regression using the Theil-Sen estimator. (**C**) Extracted growth rates were then plotted against the seeded proportion of sensitive cells in the population (i.e., $p = N_S/N_T$, where N_S is the sensitive population size and N_T is the total population size) for each well. To find the fitness functions, least square regressions (weighted against the inverse of the errors associated with each growth rate) were performed on these data. The resulting linear equations are the fitness functions $\widehat{w}_S = Ap + B(1 - p)$ and $\widehat{w}_R = Cp + D(1 - p)$. (**D**) Payoff matrices corresponding to each of the different conditions were derived from the resulting fitness functions to represent the fitness outcome of specific interactions using least square regression and intercepts of $p = 0$ and $p = 1$. For example, the fitness outcome of sensitive cells interacting with one another occurs when $p = 1$, which translates to $\widehat{w}_S = A$. Similarly, the fitness outcome of when sensitive interacts with resistant occurs when $p = 0$, which translates to $\widehat{w}_S = B$. For more details on the game assay, see (*30*) for method and (*34*) for interpretation.

increase. We can quantify this more clearly by instead plotting the gain function or the difference between the growth of the ancestor and resistant cell lines (Fig. 3B). When visualized this way, it is immediately apparent that under the treatment of DMSO, the resistant strain is competitively excluded by the sensitive strain (blue line is completely above the *x* axis). In addition, we can conclude that under the treatment of all tested gefitinib concentrations, the cell line that is outcompeted is reversed, and the sensitive strain is competitively excluded (all other lines are completely below the *x* axis). Last, we can see the slope changes from negative for DMSO to increasingly positive as the concentration of gefitinib increases. This depicts an increasing ecological interaction strength.

Competition simulations reveal the importance of ecological effects in sensitive extinction rates and tumor burden calculations

We built two kinds of mathematical models to explore the outcomes of sensitive extinction rates and tumor burden further. We extrapolated the derived fitness functions out through time using both replicator dynamics (Eq. 6) and a practical derivative of the Lotka-Volterra (LV) equation (Eq. 8) that allows for competitive exclusion of interacting species and better modeling of the time scale of extinction dynamics (*47*). Both of these models attempt to predict population trends through time. The replicator dynamics does this while modeling only frequency change and not population size (*34*). The LV model constrains the population to a strict user-chosen carrying capacity or maximum size. In vivo tumor growth likely falls somewhere in between, as nutrient availability and space constrain growth in a more fluid manner through mechanisms such as angiogenesis. For each model, relative time to extinction was determined for the range of doses, where extinction is defined as proportion of the population, *p*, falling below 0.01. As expected, both models predict faster extinction of the sensitive population at higher doses (Fig. 4, A and B).

While LV models can be quite sensitive to user-chosen carrying capacities, when the carrying capacities of both subclones are equal ($K_p = K_r = K_{max}$), heterogeneity was maintained at identical time scales when compared to the replicator equations. To evaluate the impact of frequency-dependent growth, the results were contrasted between models run with monotypic-culture growth parameters and those measured in heterotypic cultures (Fig. 4C). The model predicts that as drug concentration increases, the monotypic growth rates increasingly overestimate the time to extinction of the ancestor population

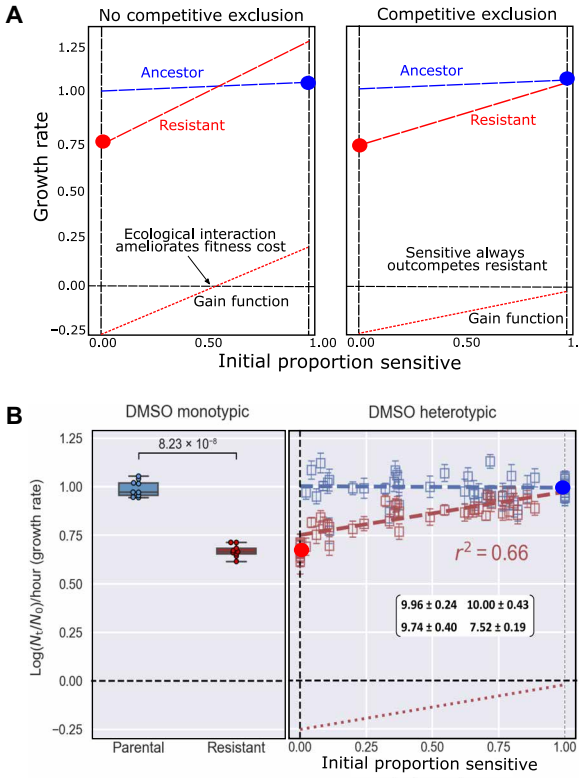

Fig. 2. Ecological interactions alter but do not ameliorate the resistant clones fitness cost and result in competitive exclusion of the resistant strain in DMSO. (**A**) Monotypic growth measurements are insufficient to predict competitive exclusion. The left and right panels both depict a resistant strain with a significant fitness cost associated with its resistance. Red circle at $p = 0$ represents monotypic resistant growth, while the blue circle at $p = 1$ represents monotypic sensitive growth. Left: We see that the ecological interaction is large enough to overcome the fitness cost when cocultured with a majority of sensitive population, resulting in no competitive exclusion. Right: While there is significant ecological interaction, it is insufficient to overcome the fitness cost, resulting in complete competitive exclusion. (**B**) Left: Monocultures in DMSO shows significant difference in growth between subclones ($p \ll 0.001$), highlighting the cost associated with the resistant phenotype. Right: Heterotypic cultures in DMSO reveal strong frequency-dependent interactions that modulate the resistant populations growth; however, these ecological forces are insufficient to completely overcome the monoculture fitness cost, leading to competitive exclusion of the resistant subclone. The ancestor's growth remains consistent at all frequencies. Plotted values were normalized against mean monotypic sensitive growth in DMSO. Values in displayed game matrix have been scaled by a factor of 10 for ease of comparison.

when compared to the more accurate heterotypic growth data. This is because the heterotypic data capture the accelerated rate of competitive exclusion that occurs as a result of ecological effects. That is, the difference between the resistant and sensitive growth rates is larger at every population fraction than the measured monotypic growth rates.

Because the assumption of equal carrying capacity may not be true of in vivo contexts, we varied the relative carrying capacity of the two population to be a ratio of the monotypic growth rates, scaled by their maximum rate in the absence of treatment (Fig. 4D). Promisingly, these results are qualitatively identical to the results gathered from using equal–carrying capacity LV models and to those predicted from replicator dynamics. However, clinical tumor burden is likely most correlated with the total tumor size and not the size of a particular subpopulation. With this in mind, we show sample time traces of total tumor population over time in response to two drug concentrations (Fig. 4E). We observe that while a lower drug concentration may lead to a smaller initial tumor decline than a larger drug concentration, the lower concentration leads to a prolonged heterogeneous, and therefore more sensitive, tumor state. This is the result of a lower dose of gefitinib prolonging the competition between ancestor and resistant populations, not allowing for a competition-free expansion by the resistant subpopulation.

Resistant lineage likely driven by *KRAS* mutation and *EGFR* down-regulation

To characterize molecular mechanisms that mediate gefitinib resistance, we then performed whole-exome and RNA sequencing, comparing resistant cells with parental and sensitive ones. Clonality inferences from genomic data indicated the polyclonal composition of ancestral cells, reflected in wide distribution of variant allele frequencies (VAFs) (Fig. 5A, top). In contrast, the distribution of VAF in resistant cells displayed two distinct peaks, centered around 0.5 and 0.3, suggesting a clonal origin of resistance with subsequent emergence of a major subclone (Fig. 5A, bottom). However, we are also aware of limitations of the presented results for clonality estimation, mainly due to copy number adjustments being relative to ancestral line and being regional estimates rather than allelic copy number estimates required for a proper cancer cell fraction (CCF) transformation; hence, we limited ourselves to a qualitative description based on the variation of transformed CCF values. Notably, resistant cells harbor clonal *KRAS G12D* mutation, which was previously shown to cause strong gefitinib resistance (*48*). Given that *KRAS G12D* is a strong oncogenic driver (*48*, *49*), this mutation likely converted PC9 cells from *EGFR* dependence to *KRAS* dependence. Consistent with this notion, resistant cells down-regulated *EGFR* expression while up-regulating the expression of *KRAS* (Fig. 5B, left, and fig. S6). In addition, we found that resistant cells displayed several copy number gains (*CCND1*, *GADD45A*, and *ARAF*) and losses (*RB1*, *FHIT*, and *AKT1*), as well as expression level changes in multiple genes (*CCND1*, *ERBB2*, and *cMET*) that have been previously linked to lung cancer progression and therapy resistance (*50*–*52*). These additional changes suggest compound-resistant phenotypes integrating impact of multiple molecular changes.

DISCUSSION

Our work provides an extensive quantitative study of the frequency-dependent interactions between an experimentally derived gefitinib-resistant PC9 cell line and its sensitive ancestor. We have shown that a fitness cost resulting from resistance may be insufficient to result in competitive exclusion of the resistant population in the absence of drug. Instead, frequency-dependent ecological interactions with the sensitive population may ameliorate the fitness cost, leading to a potential safe harbor for small resistant populations. As a result, future studies focused on competitive exclusion would benefit from an examination of frequency-dependent ecological interactions.

In addition, our work also examined how the ecological interactions may shift under increasing gefitinib doses. Our results show a shift from competitive exclusion of the resistant population to a competitive exclusion of the sensitive population as gefitinib dose is increased. Then, with simulations, we demonstrated that the inclusion of ecological effects can significantly alter calculations of sensitive

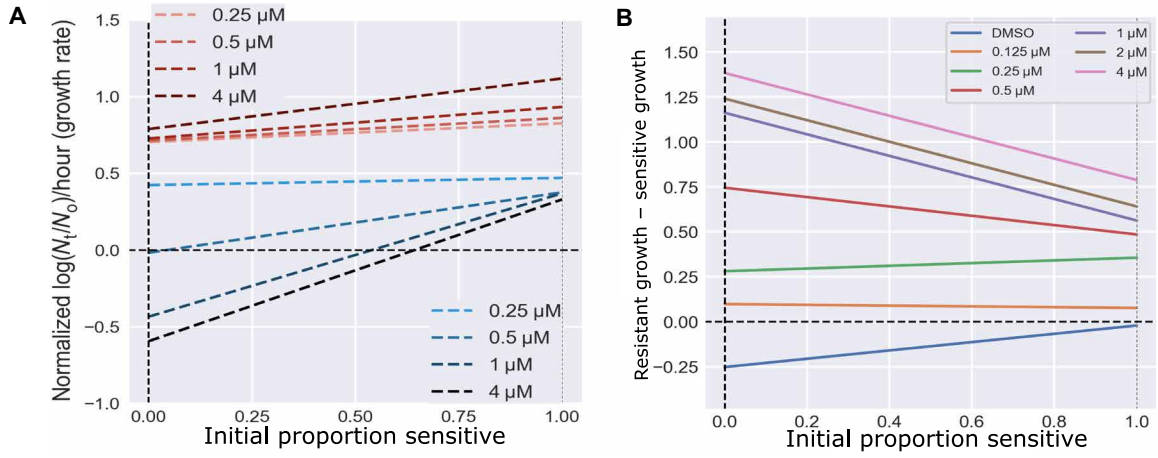

Fig. 3. Increasing gefitinib concentration switches which population is competitively excluded from resistant to ancestor. (**A**) Frequency-dependent growth rates were measured for several concentrations of gefitinib for both the gefitinib-resistant cell line (red) and the sensitive ancestor (blue). Growth values were normalized against the ancestor's mean monotypic growth in DMSO. Under all concentrations tested, we see the resistant strain outcompeting the ancestor at all population fractions, resulting in competitive exclusion of the ancestor. (**B**) Gain function (growth of resistant cell line − growth of sensitive cell line) for all seven tested concentrations of gefitinib. DMSO's (blue) gain function exists entirely above $y = 0$, signifying competitive exclusion of the resistant cell line. For all nonzero concentrations, the game dynamics shift to exist entirely below $y = 0$, indicating competitive exclusion of the sensitive strain.

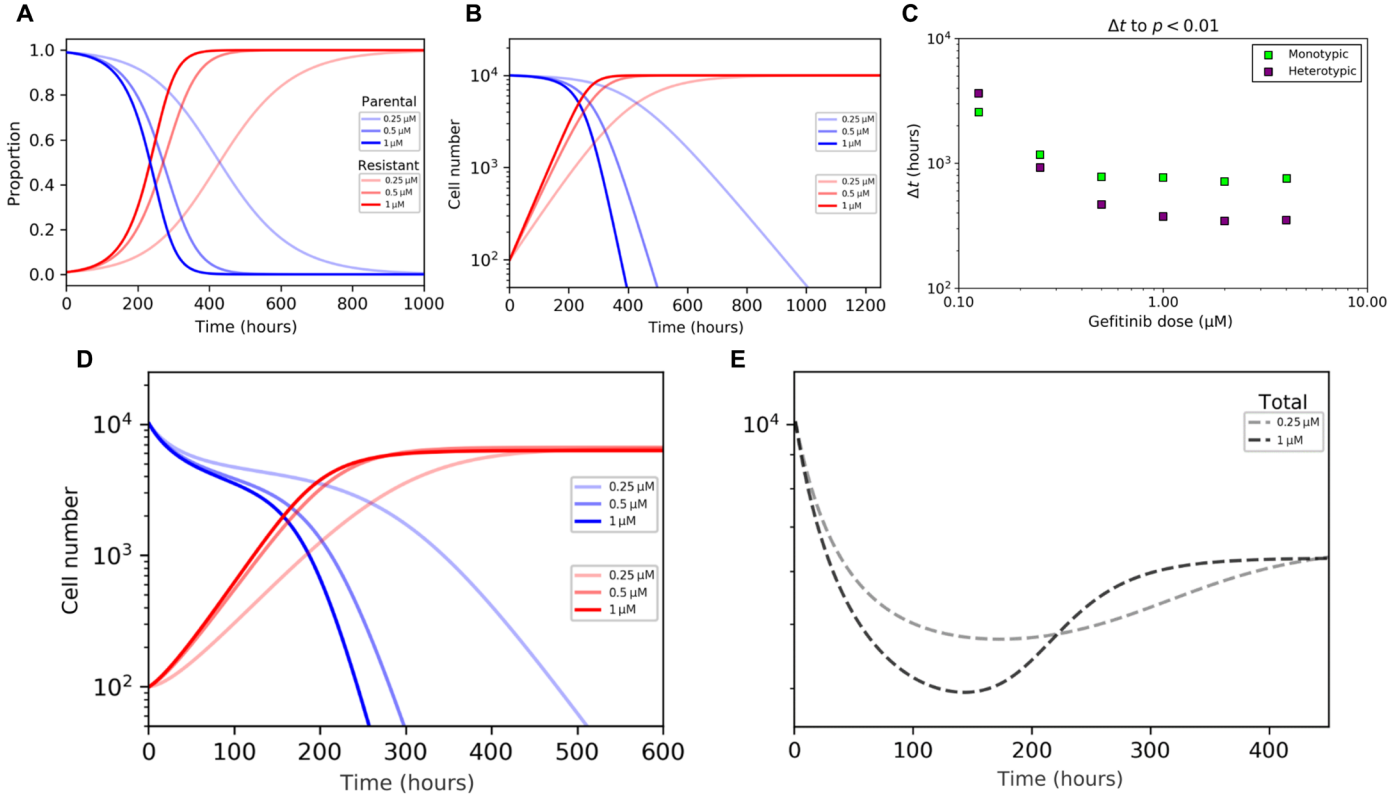

Fig. 4. Evaluation of growth models with empirically derived parameters highlights rapid acceleration of competitive release via non–cell autonomous interactions and demonstrates persistence of qualitative features across the spectrum of models tested. The same initial parameters were used for each model (parental fractions = 0.99). (**A**) Replicator dynamics showing proportional shifts of both competing cell populations over time in three gefitinib doses. (**B**) LV model of outgrowth in constrained environments with equal carrying capacities ($K_p = K_r$). (**C**) Time to extinction (defined as the proportion of the population, p, dropping below 0.01) across a range of gefitinib doses was determined and compared between cell autonomous (monotypic) and nonautonomous (heterotypic) growth. (**D**) LV model with unequal carrying capacities ($K_i = K_{max}\alpha_i$, where $\alpha_i = r_{mono}/r_{max}$). (**E**) Estimates for changes in total tumor burden for relative LV model in 0.25 and 1 μM gefitinib. Treatment with the lower dose of 0.25 μM had a smaller initial response to therapy but longer overall response due to delayed sensitive extinction and maintenance of heterogeneity over a longer period of time.

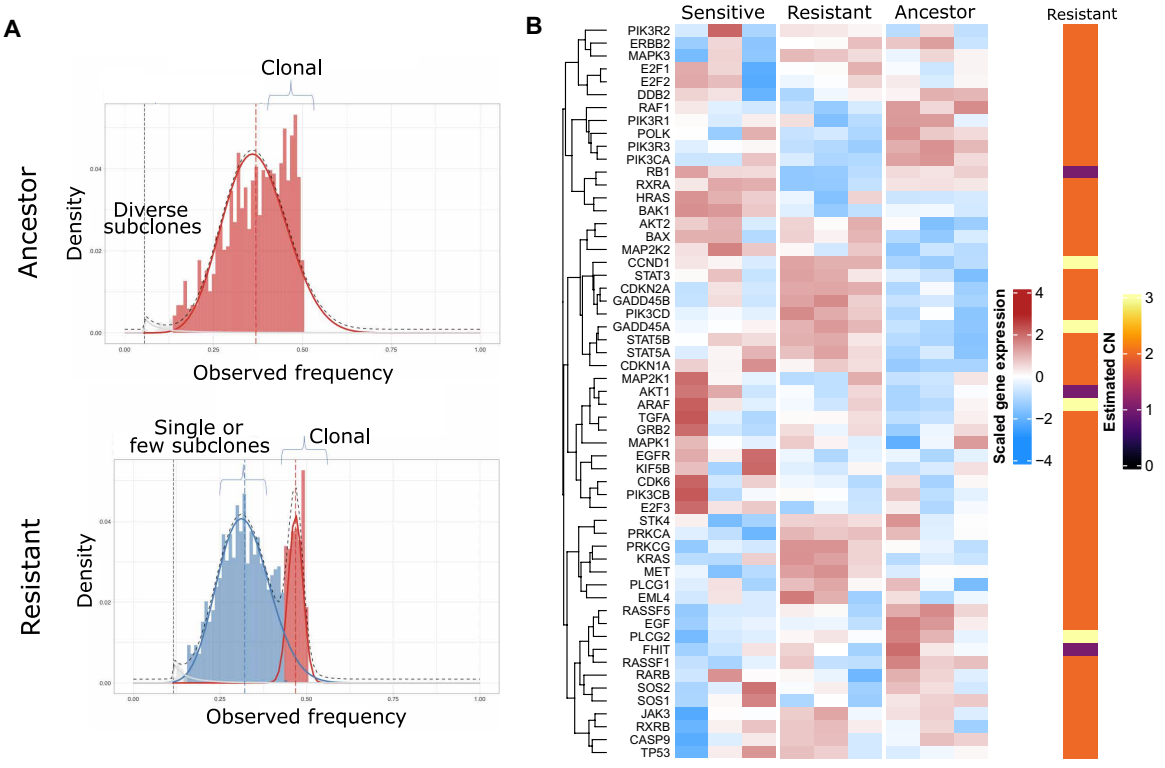

Fig. 5. Sequencing shows down-regulation of *EGFR* and up-regulation of *MET*/*KRAS* pathways in gefitinib-resistant population. (**A**) Distribution of copy number and tumor purity–adjusted VAFs suggesting heterogeneity of parental sample with a single wide peak and increased homogeneity for gefitinib-treated sample with two major narrow peaks, where a major peak near 0.5 is present, showing clonal mutations shared by the majority of the cells in the population. (**B**) Three technical replicates sampled roughly a week apart were sequenced from each of the sensitive, resistant, and parental/ancestral populations for RNA sequencing and single samples for whole-exome sequencing. CN, copy number.

extinction rate and temporal tumor burdens. Past work has shown how drug and tumor microenvironments can fluctuate in space (*53*, *54*), suggesting that these ecological interactions are likely to fluctuate over space as well. Our current work absorbs the spatial effects into the effective game measurement (*35*), but future experimental and modeling work will attempt to untangle these potential spatial contributions. Last, using whole-exome and RNA sequencing, we found that the resistant phenotype was likely driven by *KRAS G12D*, in addition to down-regulation of *EGFR* and up-regulation of *KRAS*.

In interpreting our work, several limitations are to be kept in mind. Measuring frequency-dependent ecological interactions is extremely challenging. Hence, our intention was not to produce a highly accurate clinical model of ecological interactions that can inform current cancer treatments. Instead, we focus on measuring the ecological interaction between two competing populations and how that may influence in vitro laboratory experiments. These experiments are a measurement of the interaction between one evolved gefitinib-resistant population, in coculture with a gefitinib-sensitive population. Hence, if the evolutionary process were repeated, then one may measure distinctly different ecological interactions due to the stochastic nature of evolution (*55*). In the future, we hope to measure many replicate populations to several drugs to explore the repeatability of these interactions. In addition, our experimental analysis is restricted to exponential growth phase, ignoring the effects of carry capacity and confluency that may play a significant role in similar experiments performed in mice or real-world observations in humans. In beginning to understand this more idealized scenario, we hope to understand more general principles that can be tested in more complex models of resistance and ecological interactions. With that said, it is our hope to build on this simple model to account for more complex interactions.

While our work compliments recent studies on competitive exclusion and evolutionary game theory, it also raises interesting new questions for future work. For example, clinical tumors are highly heterogeneous. Extending this work to include three (*56*) or more types will allow us to better model more clinically relevant resistance evolution. Last, our results suggest that ecological effects are an important consideration in competition experiments, and continuing to show this empirically remains a priority going forward.

METHODS

RNA-sequencing preparation

Quality control of total RNA samples is executed using Qubit Fluorometer (Invitrogen) for RNA quantification and Fragment Analyzer 5200 (Agilent) to assess RNA quality using a cutoff of RNA integrity number > 7.0 to select specimens for further analysis. The NEBNext rRNA Depletion Kit v2 (Human/Mouse/Rat) (New England Biolabs) is completed first. The rRNA-depleted RNA is used as an input for the NEBNext Ultra II Directional RNA Library Preparation Kit for Illumina (New England BioLabs) in which libraries are tagged with unique adapter indexes. Final libraries are validated on the Fragment Analyzer, quantified via quantitative polymerase chain reaction (qPCR),

and pooled at equimolar ratios. Pooled libraries are diluted, denatured, and loaded onto the Illumina NextSeq 550 system, following the NextSeq User Guide for a paired-end 75-cycle run.

Whole-exome sequencing preparation

Quality control of genomic DNA samples is executed using the Qubit dsDNA BR Assay Kit (Invitrogen, USA) and running on a 2% agarose gel. Only DNA of high quality is selected. DNA is diluted to 5 ng/μl, and a total of 50 ng of DNA is processed using the Nextera Rapid Capture Exome Kit (Illumina, San Diego, CA). This protocol starts by enzymatically shearing the DNA and tagging each sample with a unique adapter index necessary for sequencing. Final libraries are purified, quantified using the Qubit dsDNA BR Assay Kit, and pooled in sets of 12 using 500 ng of each tagged library. Each pool of libraries undergoes hybridization and targeted capture of the exome. Final library captures are validated using the Fragment Analyzer (Agilent) and quantified via qPCR (New England BioLabs). Library pools are diluted, denatured, and loaded onto the Illumina NextSeq system, following the NextSeq User Guide for a paired-end 76-cycle run.

Cell lines

All cells were cultured in RPMI 1640 medium supplemented with 10% fetal bovine serum and 1% penicillin/streptomycin. Sensitive and resistant cell lines were established from the same ancestral population of PC9 cells (Sigma-Aldrich, 90071810). Resistant population was cultured in 1 μM gefitinib (Cayman, 13166) for greater than 6 months until a population of stably growing cells was observed. Resulting subpopulations exhibited noticeable visual morphological differences in the culture. The sensitive population was cultured in parallel in matched volumes of DMSO (Sigma-Aldrich, 276855) for the same duration as a vehicle control.

Resulting resistant and sensitive subclones underwent lentiviral transduction with plasmid vectors encoding EGFP and mCherry fluorescent proteins with attached nuclear localization sequence (plasmids were a gift from A.M.'s laboratory at Moffitt Cancer Center). Derivative cell lines with heritable fluorescent protein expression were selected in puromycin (MP Biomedical, 100552).

Sequencing methods

Paired-end whole-exome sequencing reads of parental, sensitive, and resistant populations were processed to filter, align, and call variants using fastp, BWA-MEM, Strelka2, and GATK (Genome Analysis Toolkit), respectively. Read filtering with fastp included low-complexity filters followed by alignment with BWA-MEM with minimum seed length set to 17. Variant calls with Strelka2 was run using default parameters, and GATK pipeline was run according to the best-practice workflows (*57*–*59*). Variant calls passing default filters from two methods were intersected and filtered for low allelic depth. Variants are further annotated for functional consequences using Ensembl VEP (Variant Effect Predictor) tool, and associated publications are mined using LitVar (*60*, *61*). Whole-exome sequencing reads are further processed to identify copy numbers using CNVkit pipeline with default parameters and using DMSO-treated and sensitive samples to build a reference copy number profile. Copy numbers are called by default threshold values of log 2 read depth ratios (*62*). RNA sequencing quantification and analysis was done using Salmon, tximport, and edgeR tools (*63*–*65*). In addition, we generated the distribution of CCFs (scaled from 0 to 0.5); in other words, VAFs are adjusted for copy number estimates and assuming a tumor purity of 1.0 following the same "multiplicity" strategy (*66*). Scaling from 0 to 0.5 is done to represent the CCF as a pseudo VAF for input to MOBSTER package; hence, 0.5 is a proxy for clonal mutations in a diploid region (*67*). Furthermore, coupling the CCF values with MOBSTER in order to assess heterogeneity of mutations focusing on regions with high coverage, read depth of 150 is applied on variant calls across the exome (*66*). No other filtering of mutation calls is done.

Experimental design

Cells were harvested at 70 to 80% confluence, stained with trypan blue (Corning, 25-900-CI), and manually counted with a hemocytometer (Bright-Line, Z359629). Mono- and cocultures of each subclone were seeded across a range of initial relative proportions, totaling 3000 cells per well, in 96-well formats and allowed to attach for 18 to 24 hours.

Wells were treated with the following drugs: gefitinib, paclitaxel (Cayman, 10461), etoposide (Cayman, 12092), pemetrexed (Cayman, 26677), and lapatinib (Cayman, 11493) as single agents. Plates were loaded into a BioSpa 8 Automated Incubator (BioTek Instruments). Time-lapse microscopy images were obtained for bright field, GFP, and mCherry via Cytation 5 Imaging Reader (BioTek) every 4 hours over the course of 5 days.

Image processing

Images were processed with Gen5 (BioTek) and the open-source software ImageJ (*68*). Image sets were duplicated, background subtracted, contrasted using contrast limited adaptive histogram equalization (CLAHE), and thresholded. Despeckle filter was applied to the now binary images, watershed segmentation was performed, and raw cell numbers were extracted from the resulting image sets.

Evolutionary game assay

To quantify the dynamics in our in vitro environments, we used the experimental game assay developed by Kaznatcheev *et al.* (*30*). Initial proportions were calculated for each well individually from the first image. Time series of raw cell numbers were normalized against initial number in each well. Linear regression was performed using the Theil-Sen estimator on the semi-log cell change against time. The slope of the resulting linear function (with its corresponding 95% confidence interval) was translated as the growth rate across the time series, which were normalized against the average of six sensitive monoculture wells that were run on each plate.

To find the dependence of fitness on the frequency of subclonal interaction, least square regressions were performed on the growth rate against the initial proportion of sensitive cells in each well. This regression was weighted against the inverse of the errors $\left(\frac{1}{\sigma^2}\right)$ associated with each growth rate. The resulting linear equations describe fitness as a function of the initial proportion of the opposing subclone

$$\widehat{w}_P = A + \mathrm{kr} \quad (1)$$

$$\widehat{w}_R = D + \mathrm{kp} \quad (2)$$

The intercepts of these functions translate to monoculture fitness, which are the symmetric payoffs within a game matrix. The asymmetric payoffs can be translated as the fitness values when r and p are equal to 1

$$B = A + k$$
$$C = D + k$$

These linear equations can be rearranged to describe the fitness ($\widehat{w}$) of a subclone as a function of the initial proportion (p) of interacting cells within the population

$$\widehat{w}_{\mathrm{P}} = Ap + B(1-p)$$
$$\widehat{w}_{\mathrm{R}} = Cp + D(1-p)$$

Payoff matrices corresponding to each of the different conditions can be derived by setting p equal to one and zero for both equations. For example, the symmetric payoff for sensitive occurs when $p = 1$, which translates to $\widehat{w}_{\mathrm{P}} = A$

$$\begin{array}{cc} & \begin{array}{cc}\mathrm{P} & \mathrm{R}\end{array} \\ \begin{array}{c}\mathrm{P}\\ \mathrm{R}\end{array} & \begin{pmatrix} A & B \\ C & D \end{pmatrix} \end{array}$$

The errors associated with the on-diagonal payoffs are equivalent to the uncertainty of the intercept values, σ_A and σ_D, for sensitive and resistant, respectively. The errors associated with the off-diagonal payoffs were derived by propagating the uncertainty of both the intercept and the slope through both the intercept and slope of (Eq. 3)

$$\sigma_B = \sigma_A + \sigma_k \tag{3}$$

$$\sigma_C = \sigma_D + \sigma_k \tag{4}$$

Growth models

To synthesize hypothetical tumor growth using our measured frequency-dependent growth rates, we used two distinct models, one that allowed for infinite growth and one that limited total volume to a strict maximum. This was done to identify salient qualitative features that persisted across this spectrum of models, rather than make specific quantitative predictions.

For infinite growth, replicator dynamics were chosen

$$\dot{p} = p(\widehat{w}_P - \langle w \rangle) \tag{5}$$

$$\dot{r} = (1-p)(\widehat{w}_R - \langle w \rangle) \tag{6}$$

where $<w>$ denotes the average population fitness [i.e., $<w> = p\,\widehat{w}_{\mathrm{P}} + (1-p)\,\widehat{w}_{\mathrm{R}}$].

For growth that is strictly limited to a maximum, we used an LV model (*69*) with frequency-dependent growth

$$\frac{dN_p}{dt} = r_p\left[1 - \frac{N_p}{K_p} - \frac{N_r r_r}{K_p r_p}\right]N_p \tag{7}$$

$$\frac{dN_r}{dt} = r_r\left[1 - \frac{N_r}{K_r} - \frac{N_p r_p}{K_r r_r}\right]N_r \tag{8}$$

where r_p and r_r are non–cell autonomous growth rates determined by values of the game matrix such that

$$r_p = A\left(\frac{N_p}{N_p + N_r}\right) + B\left(\frac{N_r}{N_p + N_r}\right) \tag{9}$$

$$r_r = C\left(\frac{N_p}{N_p + N_r}\right) + D\left(\frac{N_r}{N_p + N_r}\right) \tag{10}$$

While this model is insensitive to specific carrying capacity values, it is highly sensitive to the relative value of the carrying capacity. Given that both subclones occupy similar space in an in vitro environment, we first evaluated the condition where the carrying capacities were equal to one another ($K_p = K_r$). This assumption likely does not translate to in vivo conditions. Instead, the carrying capacities of each type would likely vary across different environments. To capture this phenomenon, the carrying capacity was also scaled for each condition

$$K_i = K_{\max}\alpha_i \tag{11}$$

where $K_{\max}$ is the maximum carrying capacity across all conditions and α_i is a weighting term that scales this maximum using a ratio of monoculture growth rate in the current condition against the maximum growth rate $\alpha_i = \frac{r_{\mathrm{mono}}}{r_{\max}}$.

SUPPLEMENTARY MATERIALS

Supplementary material for this article is available at https://science.org/doi/10.1126/sciadv.abm7212

View/request a protocol for this paper from *Bio-protocol*.

REFERENCES AND NOTES

1. D. P. Cahill, K. W. Kinzler, B. Vogelstein, C. Lengauer, Genetic instability and darwinian selection in tumours. *Trends Cell Biol.* **9**, M57–M60 (1999).
2. L. A. Loeb, Mutator phenotype may be required for multistage carcinogenesis. *Cancer Res.* **51**, 3075–3079 (1991).
3. A. Marusyk, V. Almendro, K. Polyak, Intra-tumour heterogeneity: A looking glass for cancer? *Nat. Rev. Cancer* **12**, 323–334 (2012).
4. V. Almendro, A. Marusyk, K. Polyak, Cellular heterogeneity and molecular evolution in cancer. *Annu. Rev. Pathol.* **8**, 277–302 (2013).
5. L. A. Loeb, Human cancers express a mutator phenotype: Hypothesis, origin, and consequences. *Cancer Res.* **76**, 2057–2059 (2016).
6. N. McGranahan, C. Swanton, Biological and therapeutic impact of intratumor heterogeneity in cancer evolution. *Cancer Cell* **27**, 15–26 (2015).
7. M. Gerlinger, A. J. Rowan, S. Horswell, M. Math, J. Larkin, D. Endesfelder, E. Gronroos, P. Martinez, N. Matthews, A. Stewart, P. Tarpey, I. Varela, B. Phillimore, S. Begum, N. McDonald, A. Butler, D. Jones, K. Raine, C. Latimer, C. R. Santos, M. Nohadani, A. C. Eklund, B. Spencer-Dene, G. Clark, L. Pickering, G. Stamp, M. Gore, Z. Szallasi, J. Downward, P. A. Futreal, C. Swanton, Intratumor heterogeneity and branched evolution revealed by multiregion sequencing. *N. Engl. J. Med.* **366**, 883–892 (2012).
8. R. A. Burrell, N. McGranahan, J. Bartek, C. Swanton, The causes and consequences of genetic heterogeneity in cancer evolution. *Nature* **501**, 338–345 (2013).
9. A. Marusyk, D. P. Tabassum, P. M. Altrock, V. Almendro, F. Michor, K. Polyak, Non-cell-autonomous driving of tumour growth supports sub-clonal heterogeneity. *Nature* **514**, 54–58 (2014).
10. R. Axelrod, D. E. Axelrod, K. J. Pienta, Evolution of cooperation among tumor cells. *Proc. Natl. Acad. Sci.* **103**, 13474–13479 (2006).
11. A. M. Dujon, A. Aktipis, C. Alix-Panabières, S. R. Amend, A. M. Boddy, J. S. Brown, J.-P. Capp, J. DeGregori, P. Ewald, R. Gatenby, M. Gerlinger, M. Giraudeau, R. K. Hamede, E. Hansen, I. Kareva, C. C. Maley, A. Marusyk, N. M. Granahan, M. J. Metzger, A. M. Nedelcu, R. Noble, L. Nunney, K. J. Pienta, K. Polyak, P. Pujol, A. F. Read, B. Roche, S. Sebens, E. Solary, K. Staňková, H. S. Ewald, F. Thomas, B. Ujvari, Identifying key questions in the ecology and evolution of cancer. *Evol. Appl.* **14**, 877–892 (2021).
12. B. Wölfl, H. Te Rietmole, M. Salvioli, A. Kaznatcheev, F. Thuijsman, J. S. Brown, B. Burgering, K. Staňková, The contribution of evolutionary game theory to understanding and treating cancer. *Dyn. Games Appl.* **12**, 313–342 (2022).
13. Y. Zheng, Y. Sun, G. Torga, K. Pienta, R. Austin, Game theory cancer models of cancer cell-stromal cell dynamics using interacting particle systems. *Biophys. Rev. Lett.* **15**, 171–193 (2020).
14. A. J. Lotka, Analytical note on certain rhythmic relations in organic systems. *Proc. Natl. Acad. Sci.* **6**, 410–415 (1920).
15. S. L. Lima, Putting predators back into behavioral predator–prey interactions. *Trends Ecol. Evol.* **17**, 70–75 (2002).

16. D. Basanta, J. G. Scott, M. N. Fishman, G. Ayala, S. W. Hayward, A. R. A. Anderson, Investigating prostate cancer tumour–stroma interactions: Clinical and biological insights from an evolutionary game. *Br. J. Cancer* **106**, 174–181 (2012).
17. J. M. Pacheco, F. C. Santos, D. Dingli, The ecology of cancer from an evolutionary game theory perspective. *Interf. Focus* **4**, 20140019 (2014).
18. M. Archetti, K. J. Pienta, Cooperation among cancer cells: Applying game theory to cancer. *Nat. Rev. Cancer* **19**, 110–117 (2019).
19. K. Bohl, S. Hummert, S. Werner, D. Basanta, A. Deutsch, S. Schuster, G. Theißen, A. Schroeter, Evolutionary game theory: Molecules as players. *Mol. Biosyst.* **10**, 3066–3074 (2014).
20. A. Kaznatcheev, Evolution is exponentially more powerful with frequency-dependent selection. bioRxiv 075069 [Preprint]. 3 May 2020. https://doi.org/10.1101/2020.05.03.075069.
21. D. Basanta, R. A. Gatenby, A. R. Anderson, Exploiting evolution to treat drug resistance: Combination therapy and the double bind. *Mol. Pharm.* **9**, 914–921 (2012).
22. D. Basanta, A. R. Anderson, Exploiting ecological principles to better understand cancer progression and treatment. *Interf. Focus* **3**, 20130020 (2013).
23. M. Janiszewska, D. P. Tabassum, Z. Castaño, S. Cristea, K. N. Yamamoto, N. L. Kingston, K. C. Murphy, S. Shu, N. W. Harper, C. G. del Alcazar, M. Alečković, M. B. Ekram, O. Cohen, M. Kwak, Y. Qin, T. Laszewski, A. Luoma, A. Marusyk, K. W. Wucherpfennig, N. Wagle, R. Fan, F. Michor, S. S. McAllister, K. Polyak, Subclonal cooperation drives metastasis by modulating local and systemic immune microenvironments. *Nat. Cell Biol.* **21**, 879–888 (2019).
24. R. B. Martin, Optimal control drug scheduling of cancer chemotherapy. *Automatica* **28**, 1113–1123 (1992).
25. E. A. Yurtsev, H. X. Chao, M. S. Datta, T. Artemova, J. Gore, Bacterial cheating drives the population dynamics of cooperative antibiotic resistance plasmids. *Mol. Syst. Biol.* **9**, 683 (2013).
26. P. M. Enriquez-Navas, Y. Kam, T. Das, S. Hassan, A. Silva, P. Foroutan, E. Ruiz, G. Martinez, S. Minton, R. J. Gillies, R. A. Gatenby, Exploiting evolutionary principles to prolong tumor control in preclinical models of breast cancer. *Sci. Trans. Med.* **8**, 327ra24 (2016).
27. J. Zhang, J. J. Cunningham, J. S. Brown, R. A. Gatenby, Integrating evolutionary dynamics into treatment of metastatic castrate-resistant prostate cancer. *Nat. Commun.* **8**, 1816 (2017).
28. P. I. Warman, A. Kaznatcheev, A. Araujo, C. C. Lynch, D. Basanta, Fractionated follow-up chemotherapy delays the onset of resistance in bone metastatic prostate cancer. *Games* **9**, 19 (2018).
29. J. Maltas, K. B. Wood, Pervasive and diverse collateral sensitivity profiles inform optimal strategies to limit antibiotic resistance. *PLOS Biol.* **17**, e3000515 (2019).
30. A. Kaznatcheev, J. Peacock, D. Basanta, A. Marusyk, J. G. Scott, Fibroblasts and alectinib switch the evolutionary games played by non-small cell lung cancer. *Nat. Ecol. Evol.* **3**, 450–456 (2019).
31. Y. Viossat, R. Noble, A theoretical analysis of tumour containment. *Nat. Ecol. Evol.* **5**, 826–835 (2021).
32. M. Gluzman, J. G. Scott, A. Vladimirsky, Optimizing adaptive cancer therapy: Dynamic programming and evolutionary game theory. *Proc. R. Soc. B* **287**, 20192454 (2020).
33. J. Maltas, K. B. Wood, Dynamic collateral sensitivity profiles highlight challenges and opportunities for optimizing antibiotic sequences. bioRxiv 2021.12.19.473361 [Preprint]. 21 December 2021. https://doi.org/10.1101/2021.12.19.473361.
34. A. Kaznatcheev, Two conceptions of evolutionary games: Reductive vs effective. bioRxiv 231993 [Preprint]. 11 December 2017. https://doi.org/10.1101/231993.
35. A. Kaznatcheev, Effective games and the confusion over spatial structure. *Proc. Natl. Acad. Sci.* **115**, E1709 (2018).
36. J. West, Y. Ma, P. K. Newton, Capitalizing on competition: An evolutionary model of competitive release in metastatic castration resistant prostate cancer treatment. *J. Theor. Biol.* **455**, 249–260 (2018).
37. J. H. Connell, The influence of interspecific competition and other factors on the distribution of the Barnacle Chthamalus Stellatus. *Ecology* **42**, 710–723 (1961).
38. E. Hansen, J. Karslake, R. J. Woods, A. F. Read, K. B. Wood, Antibiotics can be used to contain drug-resistant bacteria by maintaining sufficiently large sensitive populations. *PLOS Biol.* **18**, e3000713 (2020).
39. A. R. Wargo, S. Huijben, J. C. De Roode, J. Shepherd, A. F. Read, Competitive release and facilitation of drug-resistant parasites after therapeutic chemotherapy in a rodent malaria model. *Proc. Natl. Acad. Sci.* **104**, 19914–19919 (2007).
40. S. Huijben, A. S. Bell, D. G. Sim, D. Tomasello, N. Mideo, T. Day, A. F. Read, Aggressive chemotherapy and the selection of drug resistant pathogens. *PLOS Pathog.* **9**, e1003578 (2013).
41. L. C. Pollitt, S. Huijben, D. G. Sim, R. M. Salathé, M. J. Jones, A. F. Read, Rapid response to selection, competitive release and increased transmission potential of artesunate-selected plasmodium chabaudi malaria parasites. *PLOS Pathog.* **10**, e1004019 (2014).
42. K. Bacevic, R. Noble, A. Soffar, O. Wael Ammar, B. Boszonyik, S. Prieto, C. Vincent, M. E. Hochberg, L. Krasinska, D. Fisher, Spatial competition constrains resistance to targeted cancer therapy. *Nat. Commun.* **8**, 1995 (2017).
43. G. Szakács, M. D. Hall, M. M. Gottesman, A. Boumendjel, R. Kachadourian, B. J. Day, H. Baubichon-Cortay, A. D. Pietro, Targeting the Achilles heel of multidrug-resistant cancer by exploiting the fitness cost of resistance. *Chem. Rev.* **114**, 5753–5774 (2014).
44. J. Chmielecki, J. Foo, G. R. Oxnard, K. Hutchinson, K. Ohashi, R. Somwar, L. Wang, K. R. Amato, M. Arcila, M. L. Sos, N. D. Socci, A. Viale, E. de Stanchina, M. S. Ginsberg, R. K. Thomas, M. G. Kris, A. Inoue, M. Ladanyi, V. A. Miller, F. Michor, W. Pao, Optimization of dosing for EGFR-mutant non-small cell lung cancer with evolutionary cancer modeling. *Sci. Transl. Med.* **3**, 90ra59 (2011).
45. J. Pena, L. Lehmann, G. Nöldeke, Gains from switching and evolutionary stability in multi-player matrix games. *J. Theor. Biol.* **346**, 23–33 (2014).
46. J. Karslake, J. Maltas, P. Brumm, K. B. Wood, Population density modulates drug inhibition and gives rise to potential bistability of treatment outcomes for bacterial infections. *PLOS Comput. Biol.* **12**, e1005098 (2016).
47. P. Gerlee, P. M. Altrock, Extinction rates in tumour public goods games. *J. R. Soc. Interface* **14**, 20170342 (2017).
48. M. Ali, E. Kaltenbrun, G. R. Anderson, S. J. Stephens, S. Arena, A. Bardelli, C. M. Counter, K. C. Wood, Codon bias imposes a targetable limitation on *KRAS*-driven therapeutic resistance. *Nat. Commun.* **8**, 15617 (2017).
49. C. Guerra, N. Mijimolle, A. Dhawahir, P. Dubus, M. Barradas, M. Serrano, V. Campuzano, M. Barbacid, Tumor induction by an endogenous K-ras oncogene is highly dependent on cellular context. *Cancer Cell* **4**, 111–120 (2003).
50. M. Friese-Hamim, F. Bladt, G. Locatelli, U. Stammberger, A. Blaukat, The selective c-Met inhibitor tepotinib can overcome epidermal growth factor receptor inhibitor resistance mediated by aberrant c-Met activation in NSCLC models. *Am. J. Cancer Res.* **7**, 962–972 (2017).
51. K. Erjala, M. Sundvall, T. T. Junttila, N. Zhang, M. Savisalo, P. Mali, J. Kulmala, J. Pulkkinen, R. Grenman, K. Elenius, Signaling via ErbB2 and ErbB3 associates with resistance and epidermal growth factor receptor (EGFR) amplification with sensitivity to EGFR inhibitor gefitinib in head and neck squamous cell carcinoma cells. *Clin. Cancer Res.* **12**, 4103–4111 (2006).
52. L. H. Kalish, R. A. Kwong, I. E. Cole, R. M. Gallagher, R. L. Sutherland, E. A. Musgrove, Deregulated cyclin D1 expression is associated with decreased efficacy of the selective epidermal growth factor receptor tyrosine kinase inhibitor gefitinib in head and neck squamous cell carcinoma cell lines. *Clin. Cancer Res.* **10**, 7764–7774 (2004).
53. J. G. Scott, A. B. Hjelmeland, P. Chinnaiyan, A. R. A. Anderson, D. Basanta, Microenvironmental variables must influence intrinsic phenotypic parameters of cancer stem cells to affect tumourigenicity. *PLOS Comput. Biol.* **10**, e1003433 (2014).
54. M. Kim, R. J. Gillies, K. A. Rejniak, Current advances in mathematical modeling of anti-cancer drug penetration into tumor tissues. *Front. Oncol.* **3**, 278 (2013).
55. Z. D. Blount, C. Z. Borland, R. E. Lenski, Historical contingency and the evolution of a key innovation in an experimental population of *Escherichia coli*. *Proc. Natl. Acad. Sci.* **105**, 7899–7906 (2008).
56. R. Bhattacharya, A. Mukherjee, S. Pisano, A. Altshuler, W. Nasser, S. Dey, A. Kaganovsky, A. Amitai-Lange, M. Mimouni, S. Socea, P. Hasson, C. Feral, H. Wolfenson, R. Shalom-Feuerstein, Biomechanical property of limbal niche maintains stemness through YAP. bioRxiv 2021.05.25.445490 [Preprint]. 8 May 2022. https://doi.org/10.1101/2021.05.25.445490.
57. A. McKenna, M. Hanna, E. Banks, A. Sivachenko, K. Cibulskis, A. Kernytsky, K. Garimella, D. Altshuler, S. Gabriel, M. Daly, M. A. DePristo, The Genome Analysis Toolkit: A MapReduce framework for analyzing next-generation DNA sequencing data. *Genome Res.* **20**, 1297–1303 (2010).
58. S. Kim, K. Scheffler, A. L. Halpern, M. A. Bekritsky, E. Noh, M. Källberg, X. Chen, Y. Kim, D. Beyter, P. Krusche, C. T. Saunders, Strelka2: Fast and accurate calling of germline and somatic variants. *Nat. Methods* **15**, 591–594 (2018).
59. H. Li, Aligning sequence reads, clone sequences and assembly contigs with BWA-MEM. arXiv:1303.3997 [q-bio.GN] (16 March 2013).
60. W. McLaren, L. Gil, S. E. Hunt, H. S. Riat, G. R. S. Ritchie, A. Thormann, P. Flicek, F. Cunningham, The ensembl variant effect predictor. *Genome Biol.* **17**, 122 (2016).
61. A. Allot, Y. Peng, C. H. Wei, K. Lee, L. Phan, Z. Lu, LitVar: A semantic search engine for linking genomic variant data in PubMed and PMC. *Nucleic Acids Res.* **46**, W530–W536 (2018).
62. E. Talevich, A. H. Shain, T. Botton, B. C. Bastian, CNVkit: Genome-wide copy number detection and visualization from targeted DNA sequencing. *PLOS Comput. Biol.* **12**, e1004873 (2016).
63. M. D. Robinson, D. J. McCarthy, G. K. Smyth, edgeR: A Bioconductor package for differential expression analysis of digital gene expression data. *Bioinformatics* **26**, 139–140 (2010).
64. M. I. Love, C. Soneson, M. D. Robinson, Importing transcript abundance datasets with tximport. *Dim Txi. Inf. Rep. Sample* **1**, 5 (2017).
65. R. Patro, G. Duggal, C. Kingsford, Salmon: Accurate, versatile and ultrafast quantification from RNA-seq data using lightweight-alignment. BioRxiv 021592 [Preprint] 27 June 2015. https://doi.org/10.1101/021592.
66. S. C. Dentro, D. C. Wedge, P. Van Loo, Principles of reconstructing the Subclonal architecture of cancers. *Cold Spring Harb. Perspect. Med.* **7**, a026625 (2017).

67. G. Caravagna, G. Sanguinetti, T. A. Graham, A. Sottoriva, The MOBSTER R package for tumour subclonal deconvolution from bulk DNA whole-genome sequencing data. *BMC Bioinformatics* **21**, 531 (2020).
68. J. Schindelin, I. Arganda-Carreras, E. Frise, V. Kaynig, M. Longair, T. Pietzsch, S. Preibisch, C. Rueden, S. Saalfeld, B. Schmid, J. Y. Tinevez, D. J. White, V. Hartenstein, K. Eliceiri, P. Tomancak, A. Cardona, Fiji: An open-source platform for biological-image analysis. *Nat. Methods* **9**, 676–682 (2012).
69. X.-Y. Li, C. Pietschke, S. Fraune, P. M. Altrock, T. C. G. Bosch, A. Traulsen, Which games are growing bacterial populations playing? *J. R. Soc. Interface* **12**, 20150121 (2015).

Acknowledgments: This research was supported by the Genomics Core Facility of the CWRU School of Medicine's Genetics and Genome Sciences Department and made use of the High Performance Computing Resource in the Core Facility for Advanced Research Computing at Case Western Reserve University. **Funding:** This study was supported by the National Institutes of Health (5R37CA244613-02) and the American Cancer Society Research Scholar Grant (RSG-20-096-01). **Author contributions:** Conceptualization: N.F., J.M., A.M., A.K., and J.G.S. Methodology: N.F., J.M., A.D., A.M., A.K., and J.G.S. Investigation: N.F., J.M., M.D., A.D., P.E., M.H., E.M., A.M., A.K., and J.G.S. Visualization: N.F., J.M., A.D., A.M., A.K., and J.G.S. Data scoring and analysis: N.F., J.M., A.D., and A.M. Writing (original draft): N.F., J.M., and J.G.S. Writing (review and editing): N.F., J.M., M.D., A.D., P.E., M.H., E.M., A.M., A.K., and J.G.S. Supervision: A.M., A.K., and J.G.S. **Competing interests:** The authors declare that they have no competing interests. **Data and materials availability:** All data needed to evaluate the conclusions in the paper are present in the paper and/or the Supplementary Materials. Relevant sequencing has been uploaded to the SRA with accession number: PRJNA801780.

Submitted 6 October 2021
Accepted 13 May 2022
Published 1 July 2022
10.1126/sciadv.abm7212

ScienceAdvances

Measuring competitive exclusion in non–small cell lung cancer

Nathan Farrokhian, Jeff Maltas, Mina Dinh, Arda Durmaz, Patrick Ellsworth, Masahiro Hitomi, Erin McClure, Andriy Marusyk, Artem Kaznatcheev, and Jacob G. Scott

Sci. Adv. **8** (26), eabm7212. DOI: 10.1126/sciadv.abm7212